Journal of Water Process Engineering 58 (2024) 104802

Contents lists available at ScienceDirect

Journal of Water Process Engineering

journal homepage: www.elsevier.com/locate/jwpe

A green route to the synthesis of highly porous activated carbon from walnut shells for mercury removal

Hania Albatrni [a], Ahmed Abou Elezz [b], Ahmed Elkhatat [a], Hazim Qiblawey [a,*], Fares Almomani [a]

[a] Department of Chemical Engineering, College of Engineering, Qatar University, P. O. Box 2713, Doha, Qatar
[b] Environmental Science Center, Qatar University, P.O. Box 2713, Doha, Qatar

ARTICLE INFO

Keywords:
Adsorption
Activated carbon
Potassium carbonate
Green synthesis
Chemical activation
Mercury

ABSTRACT

Activated carbon with a high surface area was synthesized using walnut shells with the objective of removing mercury ions. The procedure involved the utilization of potassium carbonate as the chemical activator. The porous material obtained was subjected to characterization using X-ray diffraction (XRD), scanning electron microscopy (SEM), Raman spectroscopy, energy-dispersive X-ray spectroscopy (EDX), Brunauer-Emmett-Teller (BET) analysis, and X-ray photoelectron spectroscopy (XPS). The BET surface areas obtained in this study reach up to 1046.9 m2/g, whereas the pore volumes range up to 0.665 cm3/g. Additionally, the findings indicate that the utilization of K_2CO_3 for chemical activation leads to the formation of a mostly amorphous structure. The present study aimed to evaluate the impact of several factors including mass dosage, pH, initial concentration of mercury, temperature, and contact time, on the efficiency of mercury removal. It was observed that the adsorption process exhibited spontaneity, endothermicity, and an increase in entropy. At a temperature of 35 °C, the adsorbent had a maximum adsorption capacity of 182.9 mg/g. The mechanism of adsorption involves the participation of ion exchange and electrostatic attractions, which combine synergistically to facilitate the process. This highlights the significance of both chemical and physical adsorption in the overall phenomenon.

1. Introduction

The accelerating growth of industrialization and sprawling urbanization in developing countries has led to water scarcity on a worldwide scale [1]. As of late, water contamination due to heavy metal ions has reached concerning levels for the environment and habitats [2]. Among heavy metal ions, mercury is a significant biologically inert and destructive metal that causes serious human detrimental effects even at low exposure levels. Exposure to this metal results in functional failure in the sensory system, kidneys, and other organs. According to the Agency for toxic substances and disease registry (ATSDR), mercury is on the "priority toxic chemicals" list. Furthermore, 128 countries signed a joint agreement during the Minamata convention to protect the environment and human health from the anthropogenic emissions of mercury originating from the cement industry, fossil fuel combustion, gold mining, paper pulp industries and electronic wastes [3] [4].

Numerous techniques have been developed to combat mercury pollution; however, further exploration is required to achieve efficient and economical solutions. Remediation methods reported in the literature include chemical oxidation, photocatalytic degradation, electrochemical degradation, membrane technologies and adsorption. Adsorption is the commonly adopted method due to its impeccable efficiency, elementary and straightforward design, formation of non-toxic by-products and low cost [5,6]. Nonetheless, a major drawback of utilizing adsorption in the industry is the high cost of purchasing commercial adsorbents. Thus, creating a hot research topic focusing on economical and more cost-effective means to develop adsorbents that are more feasible for industrial use.

Several research works for mercury removal from water have been reported in the literature. Adsorbent materials used include activated carbon (AC) [7], cryogels [8], nanomaterials [9], and biomass [10]. AC has become a very attractive option as many researchers are exploring it as a potential adsorbent for the treatment of heavy metal ions due to its active surface functional groups, high surface area, and high adsorption capacities [11–13]. However, the high cost associated with the production of AC is a drawback to its continuous use. As a means to reduce the cost of production, agricultural waste has been extensively used as precursors for the production of AC and the results proved to be comparable with that of commercial adsorbents. Many review papers have been published on the topic surrounding agricultural waste as AC

* Corresponding author.
E-mail address: hazim@qu.edu.qa (H. Qiblawey).

https://doi.org/10.1016/j.jwpe.2024.104802
Received 11 October 2023; Received in revised form 6 December 2023; Accepted 7 January 2024
Available online 17 January 2024

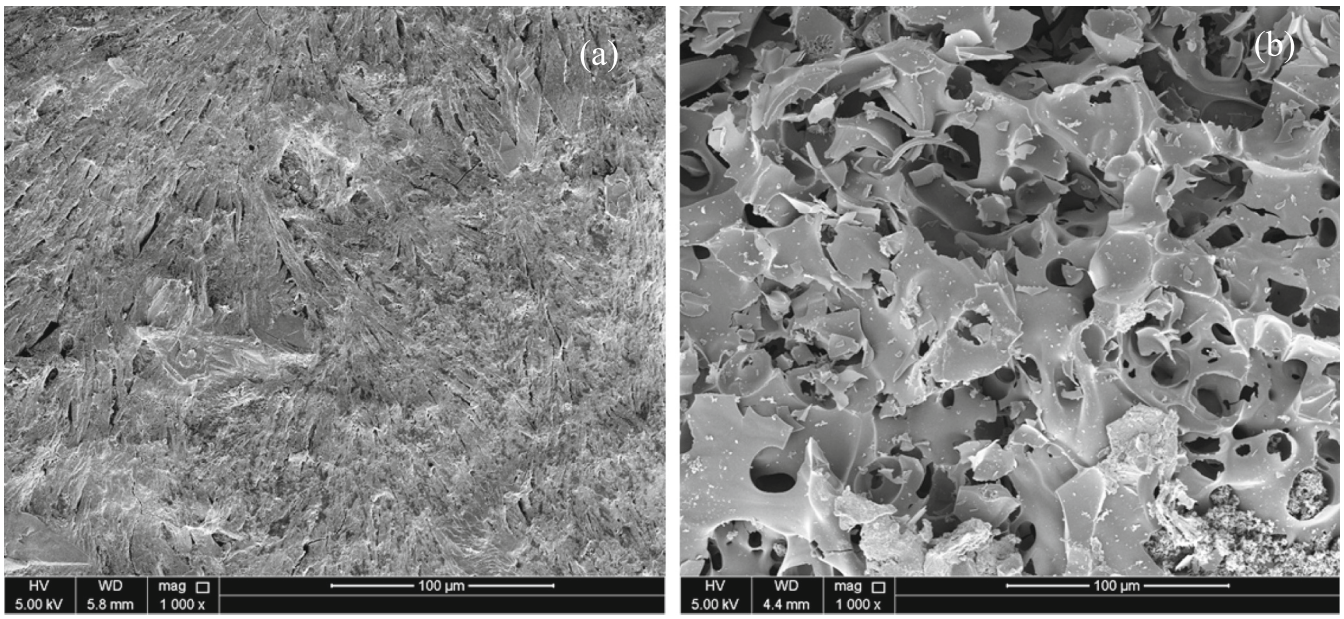

Fig. 1. SEM micrographs of WS pyrolyzed at 800 °C (a) without K_2CO_3 impregnation and (b) with K_2CO_3 impregnation.

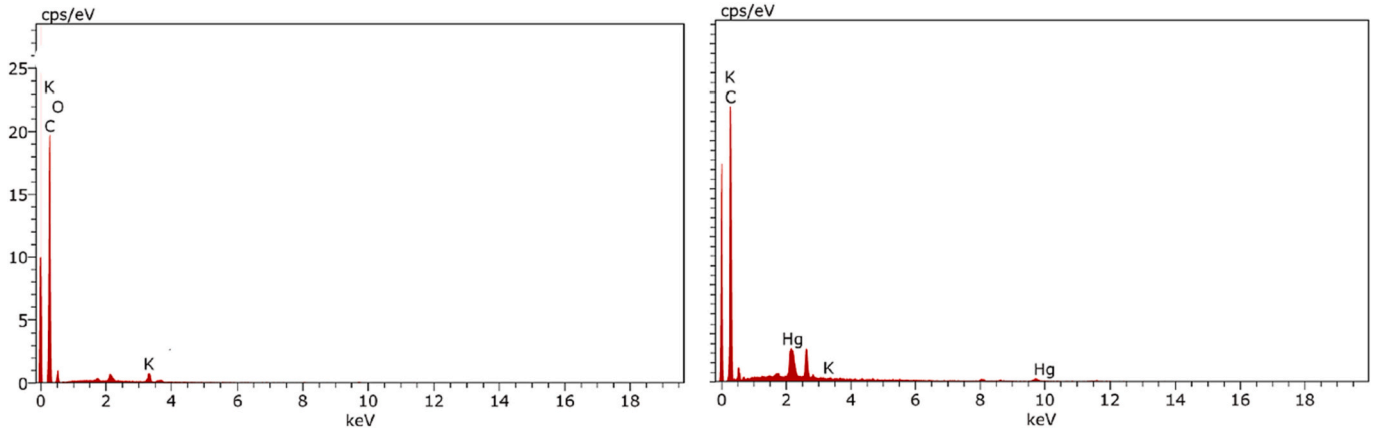

Fig. 2. EDX spectrum for WSAC before and after adsorption.

Table 1
Percentage weight of each element present in walnut shells pyrolyzed without K_2CO_3 impregnation, WSAC before adsorption and WSAC after adsorption.

Element	Pyrolysis without K_2CO_3 impregnation	Pyrolysis with K_2CO_3 impregnation (WSAC)	WSAC after adsorption
C	91.76	82.60	82.58
O	8.24	15.58	13.91
K	–	1.82	0.02
Hg	–	–	3.49

feedstock reporting very promising results. Albatrni et al. published a review on walnut shell-based adsorbents for the removal of heavy metals and organic components from aqueous solutions [14]. It was reported in the review that these agricultural waste materials exhibited prominent adsorption capacities with high specific areas and well-defined pore structures. Furthermore, walnut shells contain high carbon content and various organic and lignocellulosic compounds which is a characteristic essential in creating porous AC that in turn, leads to enhanced adsorption properties [15–17].

There are several pathways to the production of AC; however, chemical activation has been shown to produce the highest specific

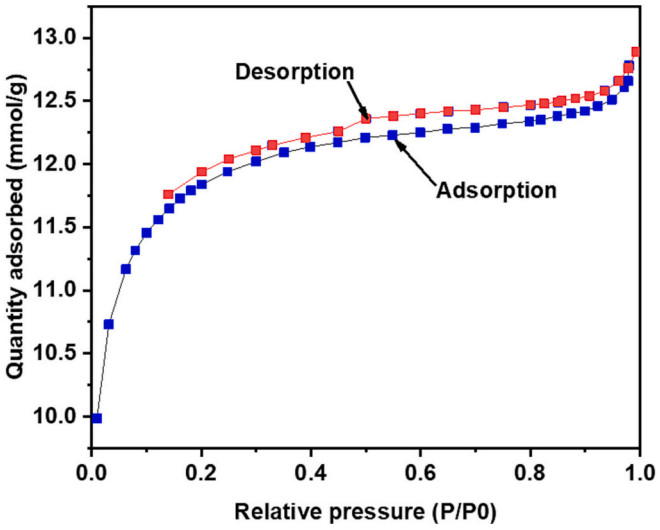

Fig. 3. N_2 adsorption/desorption isotherms for WSAC.

Table 2
Textural properties of WSAC.

BET surface area (m^2/g)	1046.9
Pore size (Å)	25.40
Langmuir surface area (m^2/g)	1873.27
Single point area (m^2/g) at P/P0 = 0.3	1241.37
Pore volume (cm^3/g)	0.665
Nanoparticle size (Å)	57.31

surface areas in addition to the effective impregnation of constitutive functional groups that are integral in the adsorption process. Liu et al. produced AC from corn cob by activating it with KOH for the removal of aqueous mercury (II) [18]. The produced AC resulted in a specific surface area of 1054.2 m^2/g. Mariana et al. experimented with candlenut shells for mercury ions removal [10]. Chemical activation was performed using NaOH at a pyrolysis temperature of 700 °C and the resulting material produced a total pore volume of 0.674 cm^3/g and a specific area of 1183 m^2/g. From the reported SEM images, activation with NaOH provided an ordered pore structure with well-developed pores indicating the significance of chemical activation. Common activating agents such as KOH, H_2SO_4, NaOH, and H_3PO_4 are all known for their detrimental effects on the environment. As of late, many are resorting to the green route approach to produce AC by employing chemical activating agents that are non-hazardous and environmentally friendly. The green route approach is an alternative synthesis route to produce AC based on harmless chemicals. Inorganic salts are non-corrosive and have the potential to produce AC with similar qualifications as AC produced with commonly used activating agents [19].

The use of walnut shells as a precursor to the production of AC is an auspicious initiative to create an economical approach focusing on the employment of low-cost renewable sources that are abundantly available. According to the Food and Agriculture Organization, the production of walnuts in 2021 was estimated to be 4.4 million metric tons with China, the USA and Iran accounting for more than two-thirds of the total global production [20] This underlines the pioneering aspect of this study in which walnut shells were carefully selected as precursors due to their lignocellulosic nature rich with organic materials and low ash content. The aim of this current study is to evaluate the potential of employing walnut shells as base waste material for the synthesis of activated carbon using K_2CO_3 as an activating agent for the removal of Hg ions from aqueous solutions and to establish optimal parameters for the adsorption process. A set of detailed experimental work and analyses are conducted to reveal adsorption mechanisms and kinetics involved in the mercury removal process.

2. Materials and methods

2.1. Materials

Mercury standard stock solution at a concentration of 1000 mg/L was obtained from Inorganic Ventures. The solution was stored at a temperature of 5 °C. Walnuts were purchased from a local market in Qatar.

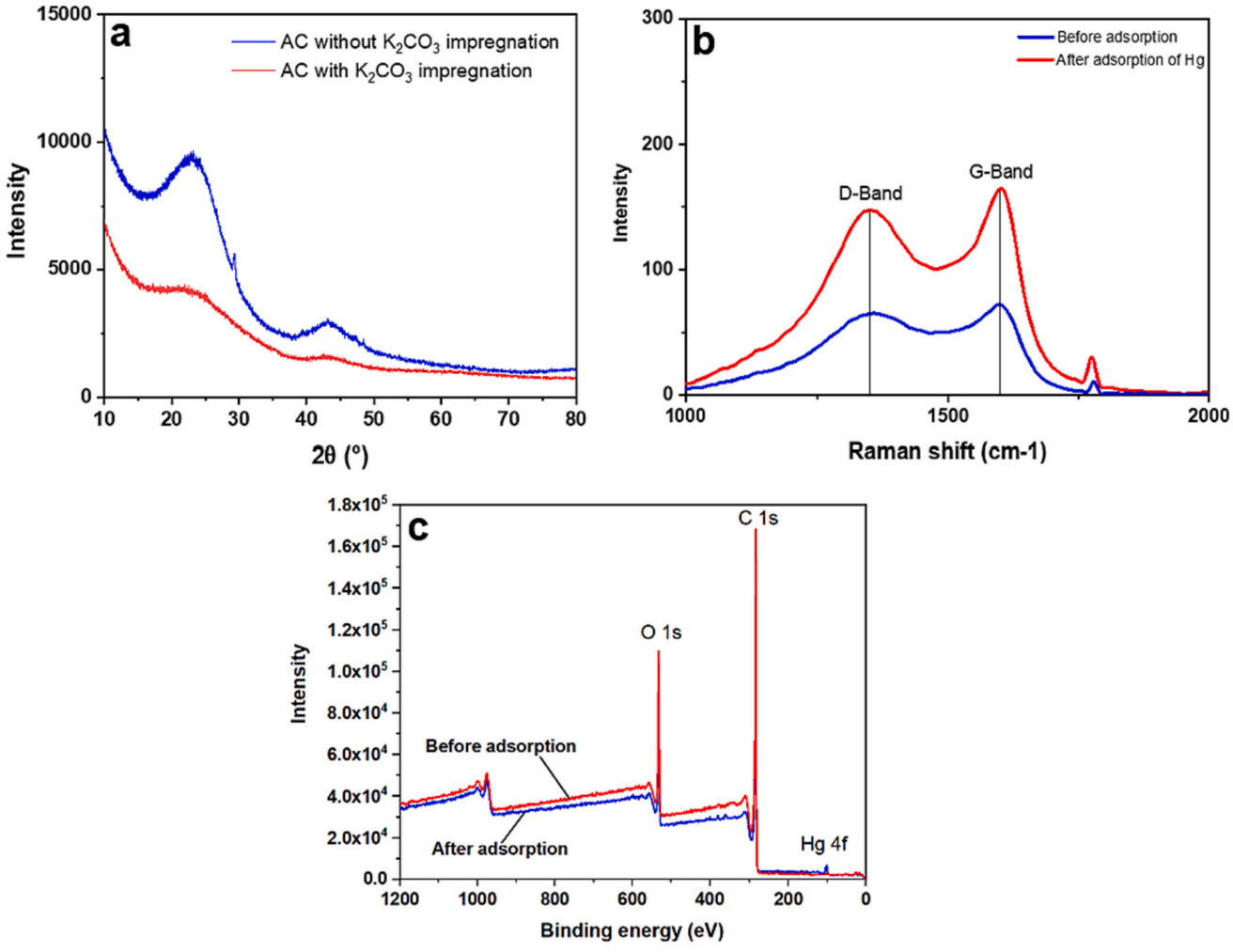

Fig. 4. XRD results of AC with and without K_2CO_3 impregnation (a) Raman spectra and (b) XPS spectra (c) of WSAC before and after adsorption.

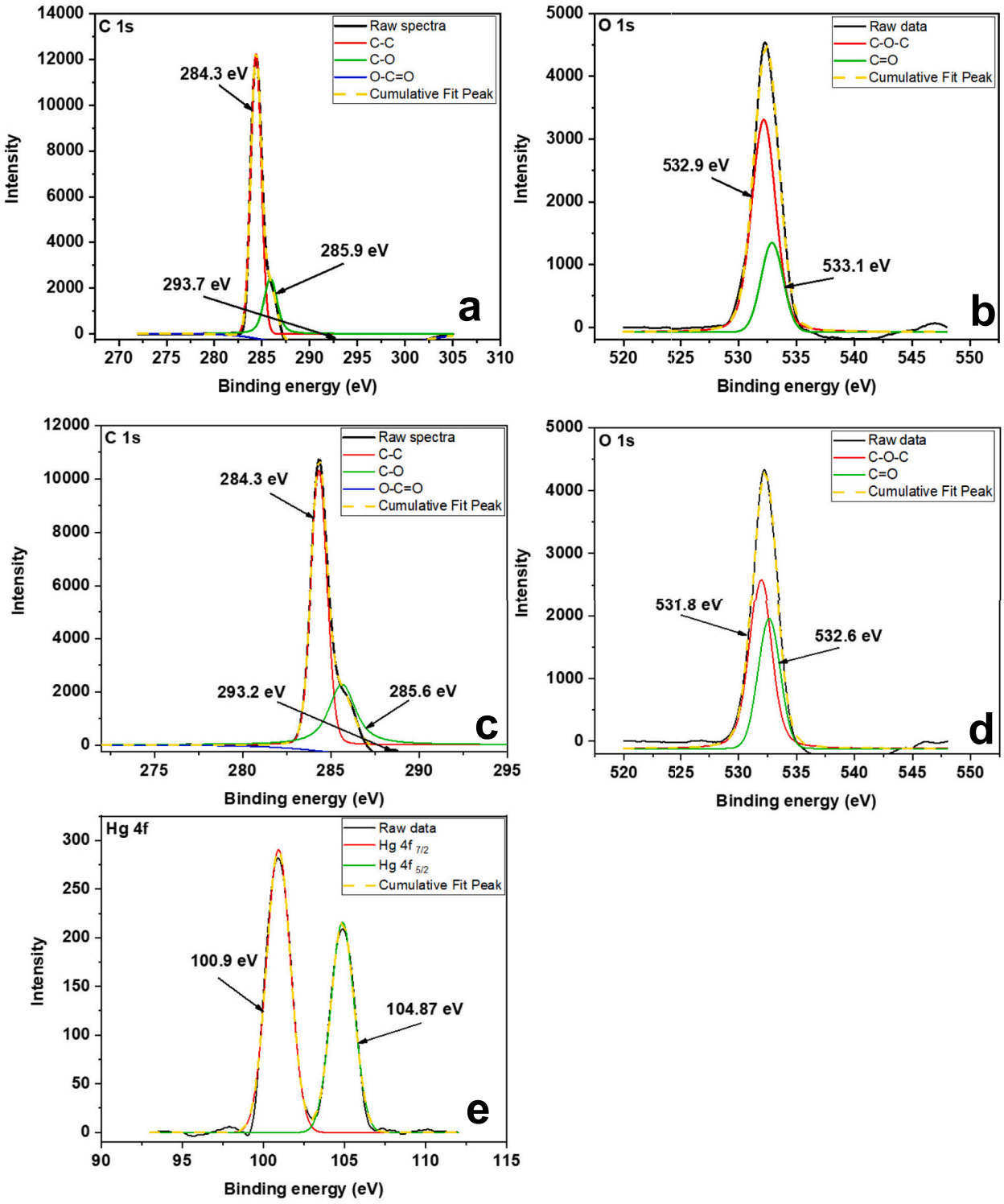

Fig. 5. XPS spectra of C 1s and O 1s before adsorption (a–b) and after adsorption (c–e).

2.2. Adsorbent preparation

Walnut shells were soaked and washed repeatedly with distilled water to remove any adhering dirt or impurities. After the washing process, walnut shells were dried at 105 °C overnight to eliminate excess moisture. Finally, the dried walnut shells were crushed and sieved to attain particles in sizes ranging from 0.8 to 1 mm.

AC's were activated through chemical activation with K_2CO_3. The precursor was placed with the activating agent at an impregnation ratio of 1:2 respectively. 10 g of K_2CO_3 was measured out and dissolved in 100 mL of distilled water. After all the potassium carbonate had been dissolved, 5 g of walnut shells were then added to the solution to achieve

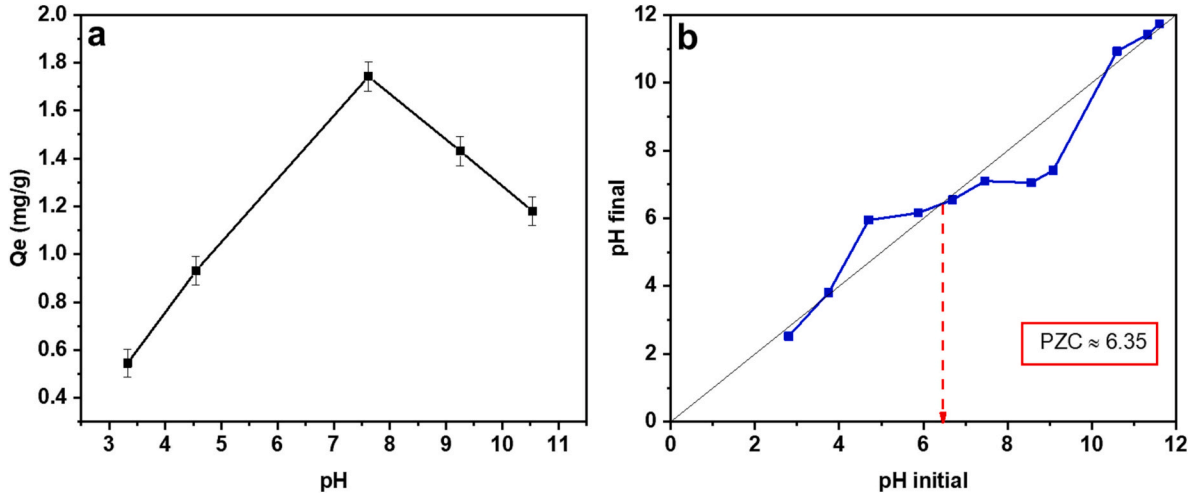

Fig. 6. pH effect on the adsorption process at room temperature, 0.01 g mass dosage, initial concentration of 10 ppm and 180 RPM (a) determination of pH point zero charge of the WSAC adsorbent (b).

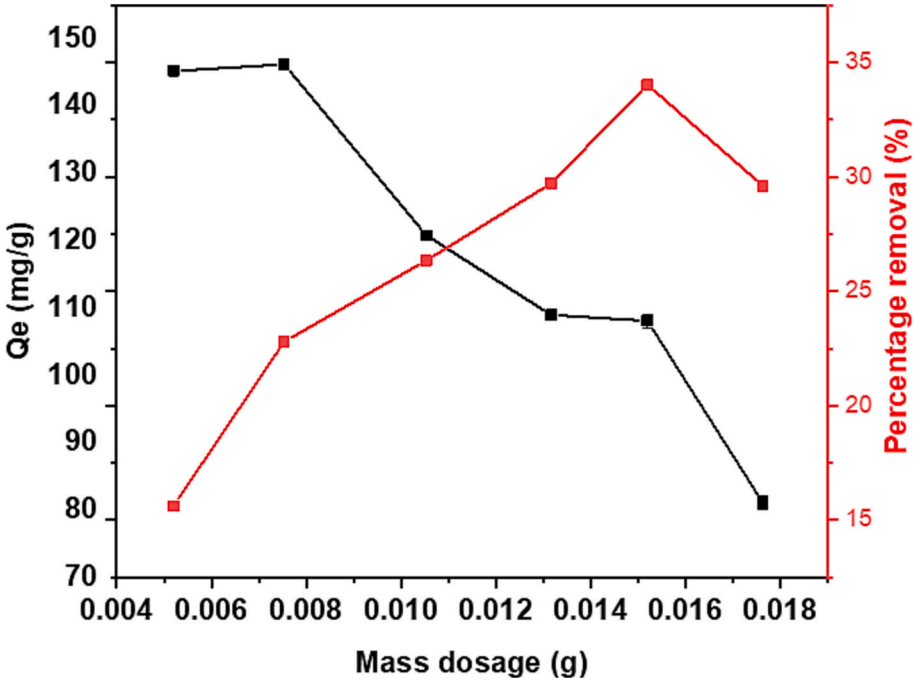

Fig. 7. The adsorbent dosage effect on the adsorption of mercury at room temperature, pH 2.3, initial concentration of 100 ppm, and 180 RPM.

solution homogeneity. The mixture was placed on a heater and stirred until all water was evaporated. The slurry was then placed at 105 °C in an oven for 24 h to ensure that the resulting mixture had completely dried. The next step is pyrolysis at inert conditions with N_2 gas being the carrier gas. Pyrolysis conditions were designed at a 5 °C/min heating rate at an N_2 flow of 100 mL/min and heating temperature of 800 °C and a stabilization time of 1 h.

Following the pyrolysis process, the samples were washed with distilled water on a stirring plate until the pH of the filtrate reached neutral conditions. Subsequently, the adsorbents were dried overnight and stored until future use.

2.3. Batch isotherm experiments

The adsorption process was assessed by evaluating the effect of four parameters. The four parameters include mercury solution concentration (5–100 mg/L), solution temperature (298–328 K), adsorbent dosage (0.005–0.0175 g) and pH (2–11). Kinetic experiments were conducted at time intervals ranging from 1 min to 24 h to identify the time at which equilibrium occurs and the maximum adsorption capacity. Batch isotherm experiments were conducted within sealed conical flasks where 50 mL of Hg solution was mixed in with the predetermined mass of adsorbent. Conical flasks were placed on a mechanical table shaker for 24 h at a speed of 180 rpm. Unless the temperature is the studied parameter, all experiments were carried out at room temperature. To evaluate the effect of pH on the adsorption process, the initial pH of the solution was altered using 1 M NaOH and 1 M HCl. Mercury ions were measured before and after the adsorption experiment using the DMA 80 direct mercury analyzer.

The adsorption capacity at time t, q_t, and percentage removal of Hg were calculated based on Eqs. (1) and (2) respectively.

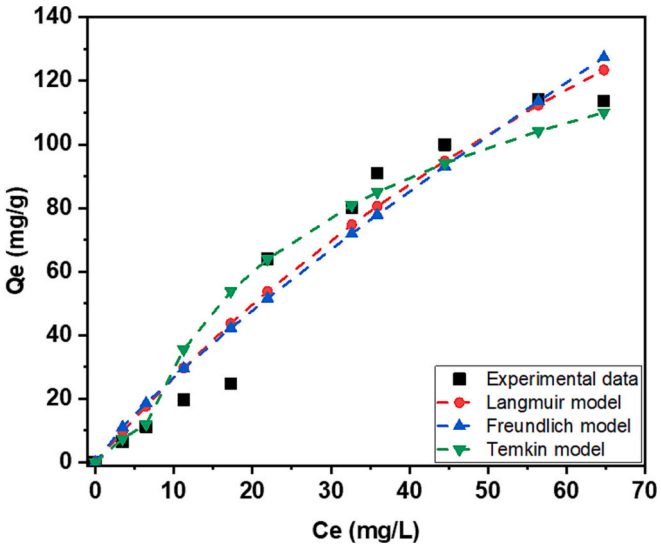

Fig. 8. Experimental data for the adsorption of Hg ions onto WSAC at 298 K and the calculated curves by non-linear adsorption isotherms of Freundlich, Langmuir, and Temkin.

$$q_t = \frac{C_0 - C_t}{m} \times V \quad (1)$$

$$\%\text{removal} = \frac{C_0 - C_t}{C_0} \times 100 \quad (2)$$

where C_0 and C_t are the initial concentration of Hg (II) ions in mg/L and at a specific time t, respectively, *m* is the mass of the adsorbent in g and V is the volume of solution in L.

2.4. Adsorbent characterization

The morphological characteristics of the adsorbent were investigated through energy-dispersive x-ray spectroscopy (EDX) and scanning electron microscopy (SEM) using Nova Nanosem 450 (Field Electron and Ion, USA). The porosity of the sample was measured by the Micrometrics ASAP2420 apparatus and it was observed from the N_2 adsorption/desorption isotherms. Crucial parameters such as the BET surface area, pore size, and total pore volume were determined using several models including BET (Brunauer-Emmett-Teller), the t-plot and BJH (Barrett-Joyner-Halenda). Samples were degassed by heating to 90 °C for 1 h, then to 350 °C for 4 h. The crystal structure was analyzed by x-ray diffraction (XRD) using the EMPYREAN model supplied by PANalytical operated at 45 kV, 40 mA using Cu anode and Kα 1 radiation (λ = 1.5406 Å). Raman scattering was conducted by employing a Thermo Fisher Scientific DXR Raman Microscope with a wavelength of 532 nm, 40 times scanning and the laser power used is 9 mW using a 50× microscope. The surface chemistry of Walnut shells activated Carbon (WSAC) was analyzed using x-ray photoelectron spectroscopy (XPS) from Escalab 250 Xi Thermo Fisher Sci. with 100 eV for survey scans and 20 eV pass energy for high-resolution scans.

3. Results and discussion

3.1. Adsorbent characterization

The SEM micrographs of the carbonized Walnut shell (WS) at 800 °C without and with activation with K_2CO_3 are displayed in Fig. 1. It is apparent from the SEM images that chemical activation has made major changes to the surface of the carbonized WS. Prior to impregnation, the surface of the WS is smooth with no visibility of pores or indents. Impregnation with K_2CO_3 disrupted the original structure of the WS creating an irregular and heterogenous surface morphology. Potassium salts are known to initiate redox reactions with carbon materials at high temperatures to yield various forms of K species including metallic K that refrain carbon layers from contracting [21]. Potassium carbonate reacts with cellulosic compounds creating penetrating cross-linked pores [22]. Thus, generating high specific areas and total pores volumes. Furthermore, metallic potassium is known to enhance pore volume and specific surface area by the action of intercalating into the carbon matrix and widening the spaces between carbon layers specifically at temperatures exceeding its boiling point (~750 °C) [23].

Fig. 2 comprises of a spectrum that has been generated by EDX analysis which corresponds to different individual elements present in the sample. Fig. 2 shows the EDX spectrum for two samples of WSAC before adsorption and after adsorption. As can be seen, potassium is

Table 3
Adsorption isotherms parameters for the adsorption of mercury onto WSAC.

Isotherms	T (C°)	Parameters			R^2	χ^2	RSME
Langmuir		K_L (L/mg)	Q_{max} (mg/g)	R_L			
ll	RT	0.0078	114.2	0.561–0.927	0.96	19.7	9.352
	35	0.0620	214.1	0.138–0.617	0.92	25.9	17.82
	45	0.1150	159.7	0.08–0.465	0.95	25.3	11.86
	55	0.0860	173.7	0.104–0.537	0.96	15.5	11.37

Isotherms	T (C°)	Parameters		R^2	χ^2	RSME
Freundlich		K_F, $L^{1/n}$ $mg^{1-1/n}$ 1/g	n			
	RT	3.91	1.19	0.95	23.4	10.49
	35	26.4	2.14	0.92	33.7	17.93
	45	42.7	2.76	0.88	54.7	18.59
	55	30.7	2.56	0.92	35.8	15.62

Isotherms	T (C°)	Parameters		R^2	χ^2	RSME
Temkin		B	A			
	RT	42.5	0.205	0.92	24.7	11.29
	35	42.7	0.818	0.92	58.6	17.86
	45	35.6	0.929	0.94	23.7	12.84
	55	34.34	1.147	0.95	27.3	12.61

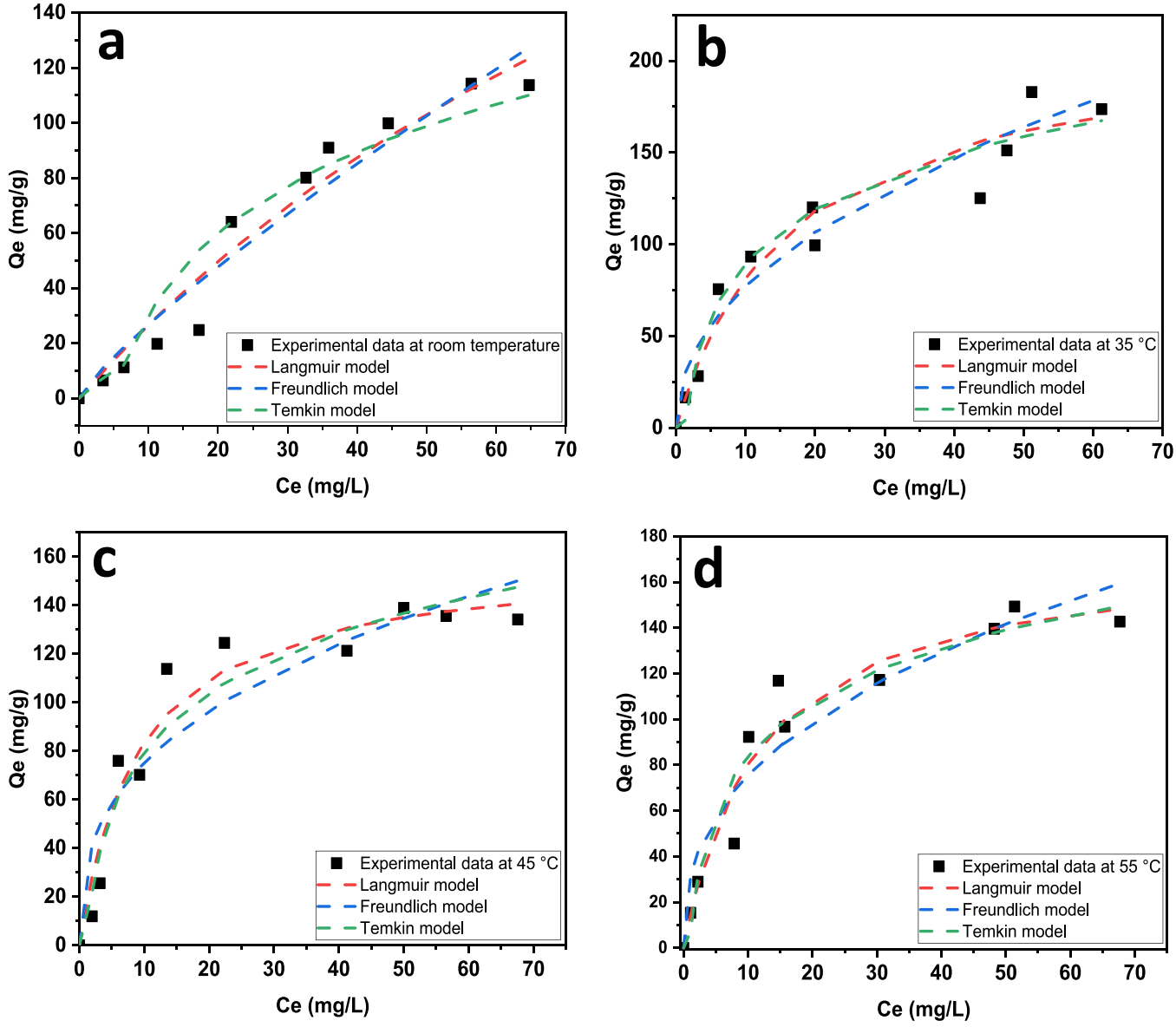

Fig. 9. Isotherm fitting into experimental data at room temperature (a) at 35 °C (b) at 45 °C (c) and 55 °C (d) at unaltered pH (pH ≈ 2), RPM of 180 and concentration range (10–100 mg/L) at 24 h. agitation time.

present in WSAC signifying the successful embedment of K in the walnut shells during the impregnation process. The potassium element has shown a reduction in its content after adsorption. This signifies that ion exchange may have occurred between mercury and potassium during the adsorption process and as a result, a decrease in K was noted in the EDX analysis results. Mercury is also present in the sample after adsorption confirming the efficacy of the adsorption process. Table 1 refers to the weight percentage of each individual element in the tested samples. This further confirms the presence of K in the sample after impregnation and the presence of mercury after the adsorption process. Walnut shells that have been pyrolyzed without K_2CO_3 impregnation were presented for comparison purposes.

The N_2 adsorption/desorption isotherm at 77 K for WSAC is presented in Fig. 3. The WSAC sample falls into the category of type I isotherm following the IUPAC classification of adsorption isotherms. This type is normally associated with micropores with a relatively small external surface area where limiting uptake is governed by accessible micropore volume as opposed to the internal surface area [24]. Moreover, a hysteresis loop is observed in the multilayer range where the two branches are horizontal and parallel over a wide range of p/p0 indicating H4 hysteresis. This type of hysteresis is often associated with narrow slit-like pores [24]. Table 2 presents the results of the BET analysis as the total pore volume of 0.665 cm^3/g and a BET surface area of the WSAC exhibited 1046.9 m^2/g. Similar findings were reported of using direct K_2CO_3 activation from materials such as the golden shower plant with BET surface area reaching 903 m^2/g [25]. The reported total pore volume and surface area (0.665 cm^3/g and1046.9 m^2/g) of the WSAC are promising and comparable with other AC produced from agricultural waste such as corn (0.674 cm^3/g and 1183 m^2/g) [10], Arun-do canes (0.56 cm^3/g and1151 m^2/g) and rice husks (1.096 cm^3/g and1180 m^2/g) [26].

The structural characteristics of the adsorbent were evaluated using XRD as shown in Fig. 4a. From the spectrum of the AC without K_2CO_3 activation, the sample exhibits a crystalline structure characterized by the presence of (002) and (010) crystal planes of the porous carbon at the angle of 2θ at 24.84° and 43.37° respectively where two prominent peaks are observed in the spectrum [27]. Chemical activation with K_2CO_3 results in broader peaks (almost disappearing) as the sample

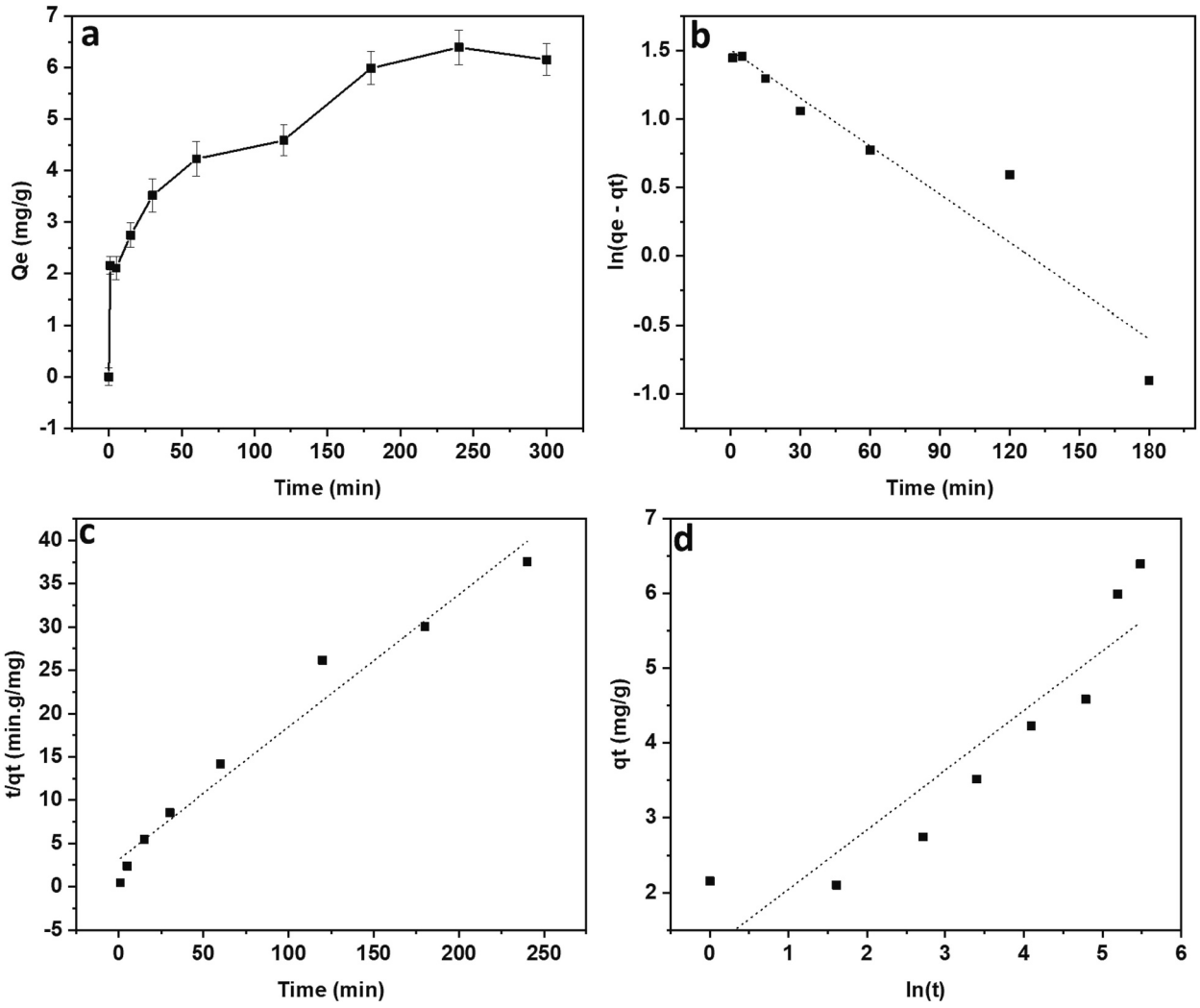

Fig. 10. Contact time experiment at room temperature, pH ≈ 2, 180 RPM (a), Pseudo-first-order model (b) Pseudo second-order model (c) and Elovich model (d).

transforms from its original crystalline structure to a predominantly amorphous structure. Fig. 4b displays the Raman spectra of WSAC before and after the adsorption process. The analyzed samples showed two characteristic bands of carbonaceous structures at ~1350 cm^{-1} and 1610 cm^{-1} which are defined as the D-band and G-band, respectively [28]. The D-band provides insight into the degree of structural disorder or structural defects, while the G-band represents graphite structures [29]. Changes in the material can be perceived from the spectra as the intensity of the bands intensified after the adsorption process presenting variation in the carbonaceous structure. The degree of defects can be identified by the relation I_D/I_G between the D- and G-bands [29]. Resulting ratios of less than one show a more ordered carbonaceous material. Ratios of I_D/I_G before and after adsorption are 0.903 and 0.892 respectively showing that the order level of the structure has been altered after adsorption. Moreover, the values indicate that the sample is an ordered carbonaceous material and has become less ordered after the adsorption process. The XPS spectra survey scan of WSAC before and after adsorption is presented in Fig. 4(c). The height of the Hg peak increased after the adsorption process conforming to the removal of mercury. When adsorption occurs on the WSAC surface, the chemical composition of the surface can be altered by either changing the chemical states of existing elements or by adding new ones. Carbon and oxygen peaks have both decreased after the adsorption process showing that new material has been adsorbed thus blocking the emission of some of the photoelectrons that would have been emitted from the underlying material. The reduction in the number of emitted photoelectrons can lead to a decrease in the intensity of the peaks in the XPS survey. Preparations of walnut shell-based AC by chemical activation with different activating agents have been reported extensively in the literature. Activation with different activation agents highly influences the characteristics of the AC. For example, SEM images acquired from AC chemically activated with K_2CO_3 form a sponge like morphology while samples impregnated with $ZnCl_2$ and H_3PO_4 yield a honeycomb-like morphology [30]. KOH has been known to produce irregular circular pore structures and activation with NaOH resulted in relatively weak pore formation [31]. Another characteristic element to include is the degree of graphitization status normally depicted by Raman spectra. Samples activated with KOH have shown similar results to the ones reported in this work where both samples have shown a graphene-like layer structure with a high degree of order [18]. To conclude, selecting the correct activating agent in the synthesis of AC is a key factor in achieving the desired results.

To further elucidate the mechanism of adsorption between mercury ions and WSAC, XPS of single elements O 1s, C 1s, and Hg 4f before and after adsorption were conducted and presented in Fig. 5. Three C 1s peaks were identified on the surface of WSAC at three binding energies 284.3, 285.9, and 293.7 eV that correspond to C—C, O—C═O, and C—O respectively [33]. As can be seen, the intensity of the peaks has decreased notably, and no noticeable shift occurred within the peaks after the adsorption process. Two O 1s peaks were detected at 532.9 and

Table 4
Kinetic parameters for the mercury adsorption onto WSAC at room temperature.

Kinetic model	Experimental data		Parameters		R^2	χ^2	RMSE
Pseudo-first order	C0 (mg/L)	Qe (mg/g)	Qe (mg/g)	K_1 (1/min)			
	1.54	6.396	4.033	0.0076	0.900	0.87	2.363
Kinetic model	Experimental data		Parameters		R^2	χ^2	RMSE
Pseudo-second order	C0 (mg/L)	Qe (mg/g)	Qe (mg/g)	K_2 (g/mg min)			
	1.54	6.396	6.531	0.00747	0.969	0.0003	0.135
Kinetic model	Experimental data		Parameters		R^2	χ^2	RMSE
Elovich	C0 (mg/L)	Qe (mg/g)	a (mg/g min)	b (g/mg)			
	1.54	6.396	0.4464	1.0725	0.948	–	–
Kinetic model	Experimental data		Parameters		R^2	χ^2	RMSE
Intraparticle diffusion	C0 (mg/L)	Qe (mg/g)	K_i	C			
	1.54	6.396	0.3057	1.664	0.9784	–	–

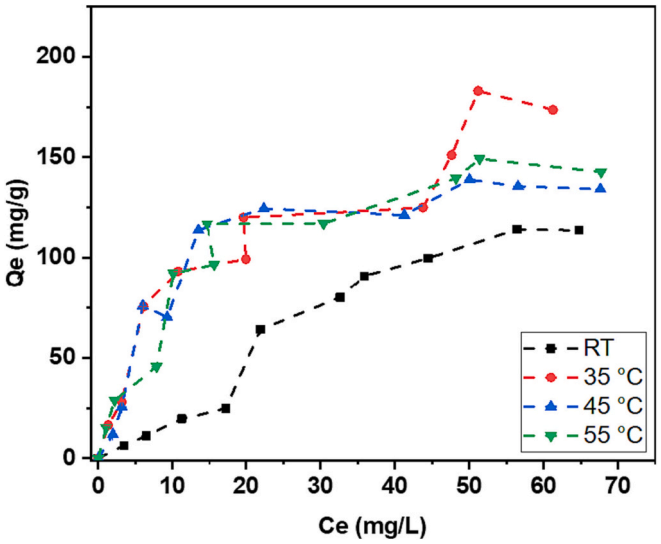

Fig. 11. Effect of temperature increase on the mercury removal onto WSAC.

Table 5
Thermodynamic parameters for the adsorption of mercury onto WSAC.

T(K)	Van't Hoff equation	K_C (–)	ΔG (kJ/mol)	ΔH° (kJ/mol)	ΔS° (J/mol K)	R^2
298		436.6	−14.80			
308	−7340.6× +	3424.8	−20.84			
318	31.48	6075.7	−23.03			
328	R2 = 0.855	5690.1	−23.57	61.03	261.7	0.855

Table 6
The adsorption capacity of different adsorbents for the removal of mercury from aqueous solutions.

Adsorbent	Operating temperature (K)	Q_{max} (mg/g)	Reference
WS chemically activation with KOH	298	269.08	[51]
Sulfurized magnetic biochar	318	70.92	[52]
Fe3O4@SiO2@PTL	318	768.25	[34]
Chitosan crosslinked with polyamine-*co*-melamine	298	140.3	[53]
Nano-magnetic AC from hazelnut shell	298	80	[39]
Magnetic sulfur-doped AC	298	187	[7]
Corn cob chemically activated by KOH	298	2.39	[18]
WSAC	308	182.9	This study

533.1 eV belonging to C═O/O—C═O groups [34]. A slight shift was observed after the adsorption process which is attributed to a shift in the electron cloud due to the presence of mercury ions [35]. Lastly, two Hg 4f peaks were registered pertaining to Hg $4f_{5/2}$ and hg $4f_{7/2}$ at binding energies at 100.9 and 104.8 eV respectively. According to this information, mercury exists in its Hg^{2+} oxidation state in the solution and that further cements the hypothesis that ion exchange may have occurred during the adsorption process involving K^+ ions.

3.2. Effect of different parameters on the adsorption process

To evaluate the adsorption performance of mercury onto WSAC, batch isotherm experiments were conducted. The effect of mass dosage, pH, initial concentration of mercury and solution temperature were examined. The impact of altering solution pH (2–12) was tested at room temperature, initial mercury concentration of 10 ppm, mass dosage of 0.01 g and agitation speed of 180 RPM, and the result is presented in Fig. 6a. The results show that the adsorption process is highly dependent on the pH. This shows that electrostatic interaction may have played a major role in the adsorption of mercury. At low pH levels, low adsorption capacities are observed after which a peak adsorption capacity is detected at pH values after 6 followed by a slight decrease in the basic region. Fig. 6b is a representation of the zero-point charge plot (pH_{ZPC}) which depicts that the surface charge of the adsorbent is close to neutral conditions as the pH_{ZPC} is close to 6.3. A neutral surface condition is an indication of a healthy balance between acidic and basic functional groups. Determining the pH_{ZPC} is a crucial step in evaluating and comprehending the adsorption performance and mechanism of WSAC on the adsorption of mercury. Steps followed to determine the pH_{ZPC} are explained by Foo et al. [36]. When the pH of the solution is below pH_{ZPC}, the surface of WSAC becomes positively charged due to protonation caused by excess H+ ions in the solution; thus, electrostatic repulsion occurs between Hg^{2+} ions and positively charged functional groups. When the pH of the solution is higher than pH_{ZPC}, the surface becomes negatively charged, hence, higher adsorption capacities are detected. A slight decrease is noted in the basic region which is due to the formation of mercury hydroxides such as $Hg(OH)_2$ or $Hg(OH)^+$ [37]. A similar finding was reported by Devasahayam et al. where AC was prepared from a mangosteen shell by chemical activation with bicarbonate [38]. Moreover, Zabihi et al. examined the pH effect on the removal of mercury using prepared nano-magnetic AC from hazelnut shell and a low adsorption capacity was reported at acidic conditions due to the presence of H+ ions which act as barriers to the active sites [39].

Fig. 7 portrays the effect of varying mass dosage of WSAC from 0.005 to 0.0175 g. Higher adsorption uptake was observed at low mass dosages and low adsorption capacities were noted at high mass dosages. This is due to the limited mercury concentration available in comparison to vacant sites available for adsorption leading to numerous vacant sites not being utilized during the adsorption process. This contributes

Table 7
Comparative study of walnut shell-based adsorbents considering optimum operational parameters.

Adsorbent	Temperature (K)	pH	Adsorbent dosage (g)	Q_{max} (Langmuir) (mg/g)	Reference
Walnut shell biochar	298	5.5	0.055	15.02	[56]
Polymer modified walnut shell	293	2–6	0.01	1250	[57]
Chemically modified walnut shells	313	2	0.01	568.18	[58]
Walnut shells modified with acrylic acid	308	6	0.0045	210.14	[59]
Walnut shells modified with diethylenetriamine	303	3	0.01	50.1	[60]
Walnut shells modified with maleic anhydride	318	5	0.16	221.24	[61]
Carboxylate functionalized walnut shells	298	5.5	0.04	192.3	[15]
WSAC	308	6.5–7.5	0.01	214.1	This study

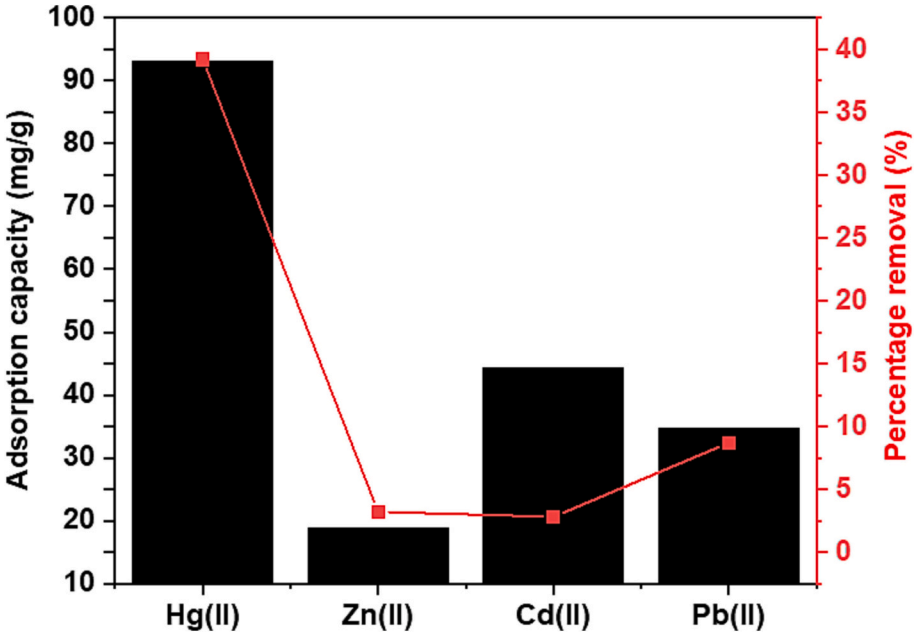

Fig. 12. Effect of competing heavy metal ions on the adsorption efficiency of Hg(II) removal.

positively and economically during the scale-up process as less amounts of the adsorbent would be needed to achieve target adsorption capacity.

3.3. Adsorption isotherms

In order to provide an adequate description of the adsorption data, three isotherm types have been applied to describe the adsorption behavior of mercury ions onto WSAC in aqueous solutions. These isotherms include Langmuir, Freundlich and Temkin isotherm models. All three isotherms were plotted and presented in Fig. 8. Isotherms parameters were determined at different operating temperatures (room temperature, 35 °C, 45 °C and 55 °C) by the non-linear optimization technique maximizing the corresponding R^2 between observed data and isotherm parameters using the Origin Pro software program and the results are presented in Table 3. The Chi-square (χ^2) function, non-linear correlation coefficient (R^2) values and root mean square error (RMSE) were taken into consideration to identify the best-fit isotherm. High χ^2 and RMSE values represent a high bias between experimental values and the model. Low χ^2 and RMSE values translate to similar data between experimental and models. From the data given in Table 3, Langmuir isotherm showed the best fitting. The highest R^2 values and the reduced χ^2 and RMSE values pertaining to the Langmuir model indicate that the Langmuir is the best fit model. Thus, it was revealed that the process is a monolayer adsorption process having equivalent activation energy among all adsorption sites. Fig. 8 depicts experimental data at room temperature along with non-linear fitted isotherms.

When employing the Langmuir isotherm to describe the adsorption process, it becomes essential to compute the separation factor. Originally, Hall et al. postulated that the fundamental attributes of the Langmuir model could be encapsulated by a dimensionless separation factor denoted as Eq. (3).

$$R_L = \frac{1}{1 + K_L C_0} \tag{3}$$

where R_L (dimensionless) is a constant separation factor for a solid-liquid adsorption system, Co (mg/L) is the initial concentration of mercury in the solution and K_L (L/mg) is the Langmuir equilibrium constant. From the separation factor, the isotherm shape was employed to deduce whether the adsorption system was favorable if $0 < R_L < 1$, unfavorable if R_L is >1, linear if $R_L = 1$ and irreversible if $R_L = 0$. All R_L values are between 0 and 1, as presented in Table 3, indicating that the isotherm shape is concave meaning that the adsorption process is favorable.

The mercury adsorption isotherms for WSAC are presented in Fig. 9 at different operating temperatures. The results have revealed that the maximum adsorption capacity is 182.9 mg/g occurring at a temperature of 35 °C, unaltered pH (≈2.1), at an agitation speed of 180 RPM. The Q_{max} obtained from the Langmuir model at the same temperature is 214.1 mg/g. This is relatively close to the experimental value. Several researchers have reported that the adsorption behavior of mercury followed the Langmuir isotherm model albeit different adsorbents of different chemical origins were employed [8,35].

3.4. Adsorption kinetics

The contact time effect on the uptake amount of mercury onto WSAC

is presented in Fig. 10a. A rapid uptake is evident from the figure during the first 30 min where >50 % of mercury was removed from the solution after which equilibrium is reached after 6 h. This behavior is ascribed to the large number of active sites available at the beginning of the experiment after which a decrease in the reaction is observed due to the occupation of these sites. Pseudo-first-order, Elovich, Pseudo-second-order, and intraparticle diffusion models were utilized in their linear form to analyze the experimental data depicted in Fig. 10b–d. The linear equations of these models are given in the supplementary data. High correlation values were obtained from all four models with Pseudo-second-order attaining the highest R^2 value. χ^2 values pertaining to both kinetic models are close to zero showing that the models are close to the experimental data. Moreover, the theoretical equilibrium adsorption capacity acquired from the Pseudo-second-order linear fit given in Table 4 is significantly close to the experimental uptake. Consequently, Pseudo-second-order was found to best describe the adsorption behavior of mercury onto WSAC. The Pseudo-second-order postulates that the adsorption process is controlled via chemisorption [42]. This proves the hypothesis that ion exchange took part during the adsorption process. According to Robalds and team members, ion exchange falls under the chemisorption process [43]. The Elovich model gave a satisfactory R^2 value and a good χ^2 value error; thus, chemisorption is not the only rate-controlling step involved in the adsorption process [25]. A plot of qt vs. $t^{0.5}$ is presented in Fig. S1 in supplementary data. A straight line with R^2 value 0f 0.978 was obtained; however, without passing through the origin. The plot interprets that intraparticle diffusion is involved in the adsorption process, however, it is not the only rate-controlling step. A multi-linear plot was observed suggesting that mercury adsorption is governed by the simultaneous occurrence of two or more mechanisms.

3.5. Adsorption thermodynamics

The effect of increasing solution temperature was assessed and portrayed in Fig. 11. From the figure, the results demonstrated that higher adsorption capacities were attained as the temperature increased to 35 °C. However, no further increase in the adsorption capacity was registered at temperatures higher than 35 °C. When the temperature increases, an enhancement in the diffusion rate occurs in the mercury molecules adsorbed on WSAC penetrate through the external boundary layer into the internal pores leading to higher adsorption rates.

A crucial step in predicting the uptake mechanisms in adsorption processes is implementing thermodynamic studies. The thermodynamic parameters are calculated according to Eq. (4). Eq. (5) presents the relationship between ΔG° with both ΔH° and ΔS°. The well-known equation of Van't Hoff is obtained by inserting Eq. (4) into (5) and presented as Eq. (6).

$$\Delta G^\circ = -RTlnK_C \tag{4}$$

$$\Delta G^\circ = \Delta H^\circ - T\Delta S^\circ \tag{5}$$

$$lnK_C = \frac{-\Delta H^\circ}{R} \times \frac{1}{T} + \frac{\Delta S^\circ}{R} \tag{6}$$

The Gibbs energy change was determined using Eq. (4). K_C is a dimensionless equilibrium constant that was computed from the Langmuir constant by multiplying K_L with the atomic weight of the adsorbate (atomic weight of mercury is 200.56 g/mol), and then by 55.5 and 1000 (number of moles of pure water per liter), an approach followed by Tran et al. [45]. Both enthalpy and entropy changes were calculated from the slope and intercept respectively. A plot of lnKc vs. 1/T was presented in Fig. S2 in the supplementary data. Calculated thermodynamic parameters are presented in Table 5. The negative values obtained pertaining to ΔG° signify that the adsorption process is spontaneous and favorable with a minimum requirement of activation energies. This is in good agreement with the separation factor analysis, R_l, where the values obtained lie between 0 and 1 suggesting the favorability of the adsorption system. In addition, Kc and ΔG° values increase with increasing investigated temperatures showing that the adsorption system is energetically favorable at high temperatures. The endothermic nature of the system is reflected in the positive value of ΔH° as can be seen in Table 5. This is also in line with the increase in adsorption capacities and constants presented in Table 3 at higher temperatures. The positive value of ΔS° demonstrates increased randomness in the system. Moreover, positive ΔS° also reveals a dissociative mechanism and the increasing degree of freedom of mercury ions in the solution. Referring to Table 5, the notably high numerical value of ΔS° implies that the adsorption process was inclined toward entropy rather than driven by enthalpy. Consequently, this led to an increase in the overall entropy within the system following the adsorption of mercury onto WSAC [25].

3.6. Adsorption mechanisms

Possible adsorption mechanisms in the heavy metal ions adsorption process involving carbonaceous materials include ion exchange, complexation, physisorption, and microprecipitation [43]. Some researchers have considered ion exchange under the umbrella of chemisorption and others have a different view and perceive it as one of the physical adsorption mechanisms. Moreover, the term electrostatic attraction or electrostatic interaction has also been suggested in the literature for the adsorption mechanism of heavy metals [43]. The pH study performed can also be utilized to gain insights into the characteristics of the adsorption mechanism. The point zero charge (PZC) is regarded as a characterization technique to verify the electrical state of an adsorbent's surface charge in solution [47]. From Fig. 6b, the PZC for the WSAC was determined to be 6.3; thus, at pH lower than pH_{PZC} WSAC is positively charged due to the protonation of the active sites which decreases gradually with pH increase [48]. As confirmed in Fig. 6a, the adsorption of cations is not favored at pH < pH_{PZC} as a result of the electrostatic repulsion between the protonated functional groups and positive mercury ions in the solution. As the pH goes beyond the pH_{PZC} the surface of WSAC becomes negatively charged initiating electrostatic attraction with the mercury ions in the solution. However, as the pH goes higher, a slight decrease is observed due to the formation of hydroxides such as $Hg(OH)_2$ and $Hg(OH)^+$ at basic conditions. Moreover, it is concluded that the adsorption mechanism involved in the process constitutes both electrostatic attraction and ion exchange. Evidence of ion exchange occurrence is seen in the decrease of potassium content on the surface of WSAC in the EDX analysis and in the interpretation of the kinetic results where the adsorption of mercury onto WSAC followed the Pseudo-second-order model which implies adsorption occurred via chemisorption. Similar results have been reported by Sun et al. for the removal of mercury using (Fe3O4@SiO2@PTL) core-shell phase-transited lysozyme film-coated magnetic nanoparticles synthesized in the lab [34].

The maximum adsorption capacity (Q_{max}) was attained by the Langmuir model at 214.1 mg/g and the experimental value obtained is 182.9 mg/g at 35 °C. The highest adsorption capacity obtained in this study was compared to others reported in the literature for the removal of mercury from aqueous solutions using different adsorbents and presented in Table 6. Furthermore, the optimum operational parameters pertaining to this study has been compared with optimum operational parameters reported by other research studies that employed walnut shells as precursors in the literature and presented in Table 7. From the table it was deduced that low adsorbent dosages and operating temperatures are required to achieve maximum adsorption capacity which is the same outcome of this research study. Also, most adsorbents were best utilized at acidic conditions and some at near neutral conditions depending on the modifying agent or activated agent; however, none were reported at basic conditions. Adsorption capacities of commercial AC have been reported in the literature. Kannan et al. investigated the removal of mercury using AC synthesized from date pits and compared it

to a commercial one [50]. The results show that AC synthesized in the lab has the potential to compete with commercial ones as the uptakes of both were 58.7 mg/g and 83.9 mg/g respectively.

3.7. Effect of competing heavy metal ions

The affinity of the WSAC toward the adsorption of Hg ions has been investigated and presented in Fig. 12. The presence of various cationic divalent ions including Zn(II), Pb(II) and Cd(II) has shown no impact on the adsorption of Hg(II) ions. Among all three heavy metals, cadmium ions may have shown that they could pose as a competing ion due to its similar divalent structure and hydrated ionic radius followed by Pb(II) ion with an uptake of 34.7 mg/g. The presence of Zn(II) almost has no effect on the adsorption of mercury with an adsorption capacity of 18.8 mg/g.

4. Conclusions

The chemical activation method using K_2CO_3 using walnut shells as precursor was successfully implemented. The synthesized adsorbent, WSAC, has proved to be an effective adsorbent for the removal of mercury from aqueous solutions. The BET surface area was determined to be 1046.9 m^2/g and the total pore volume of 0.665 cm^3/g which is comparable with those reported in the literature. A maximum adsorption capacity of 182.9 mg/g at 35 °C, pH of 2.3, mass dosage of 0.01 g and 180 RPM confirms the efficacy of the adsorbent. The adsorption process was best described using the Langmuir isotherm model and Pseudo-second-order kinetic model. From the thermodynamics study, it was elucidated that the adsorption of mercury onto WSAC was endothermic in nature and spontaneous. The adsorption mechanism encompasses the involvement of ion exchange and electrostatic attractions, which work together synergistically to enhance the process. This underscores the importance of both chemical and physical adsorption in the overarching phenomenon. Thus, this research work not only portrayed the efficiency of this adsorbent but also paved the path for a green and low-cost adsorbent that can be utilized in the industry.

CRediT authorship contribution statement

Hania Albatrni: Formal analysis, Methodology, Writing – original draft. **Ahmed Abou Elezz:** Formal analysis, Writing – review & editing. **Ahmed Elkhatat:** Formal analysis, Writing – review & editing. **Hazim Qiblawey:** Conceptualization, Funding acquisition, Methodology, Supervision, Writing – review & editing. **Fares Almomani:** Formal analysis, Writing – review & editing.

Declaration of competing interest

The authors declare that they have no known competing financial interests or personal relationships that could have appeared to influence the work reported in this paper.

Data availability

Data will be made available on request.

Acknowledgment

Financial support through the internal grant (QUCG-CENG-23/24-111) by Qatar University is acknowledged. Open Access funding is provided by the Qatar National Library. The support received from QU central laboratory units (CLU) throughout the duration of this research project is acknowledged, too.

Appendix A. Supplementary data

Supplementary data to this article can be found online at https://doi.org/10.1016/j.jwpe.2024.104802.

References

[1] D. Ewis, A. Benamor, M.M. Ba-Abbad, M. Nasser, M. El-Naas, H. Qiblawey, Removal of oil content from oil-water emulsions using iron oxide/bentonite nano adsorbents, J. Water Process Eng. 38 (2020) 101583, https://doi.org/10.1016/J.JWPE.2020.101583.
[2] R. Black, M. Sartaj, A. Mohammadian, H.A.M. Qiblawey, Biosorption of Pb and Cu using fixed and suspended bacteria, J. Environ. Chem. Eng. 2 (2014) 1663–1671, https://doi.org/10.1016/J.JECE.2014.05.023.
[3] B. Moossa, H. Qiblawey, M.S. Nasser, M.A. Al-Ghouti, A. Benamor, Electronic waste considerations in the Middle East and North African (MENA) region: a review, Environ. Technol. Innov. 29 (2023) 102961, https://doi.org/10.1016/J.ETI.2022.102961.
[4] L.J. Esdaile, J.M. Chalker, The mercury problem in artisanal and small-scale gold mining, Chem. Eur. J. 24 (2018) 6905–6916, https://doi.org/10.1002/chem.201704840.
[5] H. Albatrni, H. Qiblawey, M.H. El-Naas, Comparative study between adsorption and membrane technologies for the removal of mercury, Sep. Purif. Technol. 257 (2021), https://doi.org/10.1016/j.seppur.2020.117833.
[6] T. Alomar, H. Qiblawey, F. Almomani, R.I. Al-Raoush, D.S. Han, N.M. Ahmad, Recent advances on humic acid removal from wastewater using adsorption process, J. Water Process Eng. 53 (2023) 103679, https://doi.org/10.1016/J.JWPE.2023.103679.
[7] B. Zhang, S. Petcher, H. Gao, P. Yan, D. Cai, G. Fleming, D.J. Parker, S.Y. Chong, T. Hasell, Magnetic sulfur-doped carbons for mercury adsorption, J. Colloid Interface Sci. 603 (2021) 728–737, https://doi.org/10.1016/j.jcis.2021.06.129.
[8] A.Z. Baimenov, D.A. Berillo, K. Moustakas, V.J. Inglezakis, Efficient removal of mercury (II) from water by use of cryogels and comparison to commercial adsorbents under environmentally relevant conditions, J. Hazard. Mater. 399 (2020), https://doi.org/10.1016/j.jhazmat.2020.123056.
[9] H. Khurshid, M.R.U. Mustafa, M.H. Isa, Adsorption of chromium, copper, lead and mercury ions from aqueous solution using bio and nano adsorbents: a review of recent trends in the application of AC, BC, nZVI and MXene, Environ. Res. 212 (2022), https://doi.org/10.1016/j.envres.2022.113138.
[10] M. Mariana, E.M. Mistar, M. Syabriyana, A.S. Zulkipli, D. Aswita, T. Alfatah, Properties and adsorptive performance of candlenut shell and its porous charcoals for aqueous mercury(II) removal, Bioresour. Technol. Rep. 19 (2022), https://doi.org/10.1016/j.biteb.2022.101182.
[11] N.A. Rashidi, S. Yusup, A review on recent technological advancement in the activated carbon production from oil palm wastes, Chem. Eng. J. 314 (2017) 277–290, https://doi.org/10.1016/J.CEJ.2016.11.059.
[12] O. Ioannidou, A. Zabaniotou, Agricultural residues as precursors for activated carbon production—a review, Renew. Sust. Energ. Rev. 11 (2007) 1966–2005, https://doi.org/10.1016/J.RSER.2006.03.013.
[13] R. Yousef, H. Qiblawey, M.H. El-Naas, Adsorption as a process for produced water treatment: a review, Processes 8 (2020) 1–22, https://doi.org/10.3390/pr8121657.
[14] H. Albatrni, H. Qiblawey, M.J. Al-Marri, Walnut shell based adsorbents: a review study on preparation, mechanism, and application, J. Water Process Eng. 45 (2022), https://doi.org/10.1016/j.jwpe.2021.102527.
[15] M. Ashrafi, H. Borzuie, G. Bagherian, M.A. Chamjangali, H. Nikoofard, Artificial neural network and multiple linear regression for modeling sorption of Pb2+ ions from aqueous solutions onto modified walnut shell, Sep. Sci. Technol. (Phila.) 55 (2020) 222–233, https://doi.org/10.1080/01496395.2019.1577437.
[16] Z. Li, H. Hanafy, L. Zhang, L. Sellaoui, M. Schadeck Netto, M.L.S. Oliveira, M. K. Seliem, G. Luiz Dotto, A. Bonilla-Petriciolet, Q. Li, Adsorption of congo red and methylene blue dyes on an ashitaba waste and a walnut shell-based activated carbon from aqueous solutions: experiments, characterization and physical interpretations, Chem. Eng. J. 388 (2020), https://doi.org/10.1016/j.cej.2020.124263.
[17] X. Liang, B. Liang, J. Wei, S. Zhong, R. Zhang, Y. Yin, Y. Zhang, H. Hu, Z. Huang, A cellulose-based adsorbent with pendant groups of quaternary ammonium and amino for enhanced capture of aqueous Cr(VI), Int. J. Biol. Macromol. 148 (2020) 802–810, https://doi.org/10.1016/J.IJBIOMAC.2020.01.184.
[18] Z. Liu, Y. Sun, X. Xu, X. Meng, J. Qu, Z. Wang, C. Liu, B. Qu, Preparation, characterization and application of activated carbon from corn cob by KOH activation for removal of Hg(II) from aqueous solution, Bioresour. Technol. 306 (2020), https://doi.org/10.1016/j.biortech.2020.123154.
[19] Y. Sun, G. Yang, Y.S. Wang, J.P. Zhang, Production of activated carbon by K 2CO 3 activation treatment of furfural production waste and its application in gas storage, Environ. Prog. Sustain. Energy 30 (2011) 648–657, https://doi.org/10.1002/ep.10503.
[20] C.S.G.P. Queirós, S. Cardoso, A. Lourenço, J. Ferreira, I. Miranda, M.J.V. Lourenço, H. Pereira, Characterization of walnut, almond, and pine nut shells regarding chemical composition and extract composition, Biomass Convers. Biorefin. 10 (2020) 175–188, https://doi.org/10.1007/s13399-019-00424-2.
[21] G. Singh, A. Maria Ruban, X. Geng, A. Vinu, Recognizing the potential of K-salts, apart from KOH, for generating porous carbons using chemical activation, Chem. Eng. J. 451 (2023), https://doi.org/10.1016/j.cej.2022.139045.

[22] P. Nowicki, J. Kazmierczak-Razna, R. Pietrzak, Physicochemical and adsorption properties of carbonaceous sorbents prepared by activation of tropical fruit skins with potassium carbonate, Mater. Des. 90 (2016) 579–585, https://doi.org/10.1016/j.matdes.2015.11.004.
[23] H. Arslanoğlu, Direct and facile synthesis of highly porous low cost carbon from potassium-rich wine stone and their application for high-performance removal, J. Hazard. Mater. 374 (2019) 238–247, https://doi.org/10.1016/J.JHAZMAT.2019.04.042.
[24] D.W. McKee, Mechanisms of the alkali metal catalysed gasification of carbon, Fuel 62 (1983) 170–175, https://doi.org/10.1016/0016-2361(83)90192-8.
[25] H.N. Tran, S.J. You, H.P. Chao, Fast and efficient adsorption of methylene green 5 on activated carbon prepared from new chemical activation method, J. Environ. Manag. 188 (2017) 322–336, https://doi.org/10.1016/J.JENVMAN.2016.12.003.
[26] E. Menya, P.W. Olupot, H. Storz, M. Lubwama, Y. Kiros, Production and performance of activated carbon from rice husks for removal of natural organic matter from water: a review, Chem. Eng. Res. Des. 129 (2018) 271–296, https://doi.org/10.1016/J.CHERD.2017.11.008.
[27] A. Alkhouzaam, H. Qiblawey, M. Khraisheh, Polydopamine functionalized graphene oxide as membrane nanofiller: spectral and structural studies, Membranes (Basel) 11 (2021) 1–17, https://doi.org/10.3390/membranes11020086.
[28] A. Alkhouzaam, H. Qiblawey, M. Khraisheh, M. Atieh, M. Al-Ghouti, Synthesis of graphene oxides particle of high oxidation degree using a modified Hummers method, Ceram. Int. 46 (2020) 23997–24007, https://doi.org/10.1016/J.CERAMINT.2020.06.177.
[29] S. Giraldo, I. Robles, A. Ramirez, E. Flórez, N. Acelas, Mercury removal from wastewater using agroindustrial waste adsorbents, SN Appl. Sci. 2 (2020), https://doi.org/10.1007/s42452-020-2736-x.
[30] M. Kiliç, E. Apaydin-Varol, A.E. Pütün, Preparation and surface characterization of activated carbons from *Euphorbia rigida* by chemical activation with ZnCl 2 , K 2 CO 3 , NaOH and H 3 PO 4, Appl. Surf. Sci. 261 (2012) 247–254, https://doi.org/10.1016/j.apsusc.2012.07.155.
[31] Z. Liu, Y. Sun, X. Xu, J. Qu, B. Qu, Adsorption of Hg(II) in an aqueous solution by activated carbon prepared from rice husk using KOH activation, ACS Omega 5 (2020) 29231–29242, https://doi.org/10.1021/acsomega.0c03992.
[33] H.H. Kim, T.G. Lee, Removal of mercury ions in a simulated wastewater using functionalized poly(glycidyl methacrylate), J. Ind. Eng. Chem. 47 (2017) 446–450, https://doi.org/10.1016/J.JIEC.2016.12.019.
[34] Y. Sun, X. Li, W. Zheng, Facile synthesis of core-shell phase-transited lysozyme coated magnetic nanoparticle as a novel adsorbent for Hg(II) removal in aqueous solutions, J. Hazard. Mater. 403 (2021), https://doi.org/10.1016/j.jhazmat.2020.124012.
[35] H. Zhu, C. Ni, L. Zhou, Y. Chen, Y. Qin, Facile synthesis of multifunctional acylhydrazone-based covalent organic polymer for rapid removing Hg(II) and Ibuprofen from water, J. Environ. Chem. Eng. 11 (2023), https://doi.org/10.1016/j.jece.2022.109228.
[36] K.Y. Foo, B.H. Hameed, Adsorption characteristics of industrial solid waste derived activated carbon prepared by microwave heating for methylene blue, Fuel Process. Technol. 99 (2012) 103–109, https://doi.org/10.1016/j.fuproc.2012.01.031.
[37] M. Yin, X. Bai, D. Wu, F. Li, K. Jiang, N. Ma, Z. Chen, X. Zhang, L. Fang, Sulfur-functional group tunning on biochar through sodium thiosulfate modified molten salt process for efficient heavy metal adsorption, Chem. Eng. J. 433 (2022), https://doi.org/10.1016/j.cej.2021.134441.
[38] A. Devasahayam, R.A. Ramanujam, S. Ramasamy, Modified Mangosteen Shell in the Removal of Hg (II) From Aqueous Solution-isotherm and Kinetic Studies. http://epg.science.cmu.ac.th/ejournal/, 2020.
[39] M. Zabihi, M. Omidvar, A. Motavalizadehkakhky, R. Zhiani, Competitive adsorption of arsenic and mercury on nano-magnetic activated carbons derived from hazelnut shell, Korean J. Chem. Eng. 39 (2022) 367–376, https://doi.org/10.1007/s11814-021-0903-4.
[42] J. He, Y. Lu, G. Luo, Ca(II) imprinted chitosan microspheres: an effective and green adsorbent for the removal of Cu(II), Cd(II) and Pb(II) from aqueous solutions, Chem. Eng. J. 244 (2014) 202–208, https://doi.org/10.1016/J.CEJ.2014.01.096.
[43] A. Robalds, G.M. Naja, M. Klavins, Highlighting inconsistencies regarding metal biosorption, J. Hazard. Mater. 304 (2016) 553–556, https://doi.org/10.1016/j.jhazmat.2015.10.042.
[45] H.N. Tran, S.J. You, H.P. Chao, Thermodynamic parameters of cadmium adsorption onto orange peel calculated from various methods: a comparison study, J. Environ. Chem. Eng. 4 (2016) 2671–2682, https://doi.org/10.1016/J.JECE.2016.05.009.
[47] H.N. Tran, S.J. You, A. Hosseini-Bandegharaei, H.P. Chao, Mistakes and inconsistencies regarding adsorption of contaminants from aqueous solutions: a critical review, Water Res. 120 (2017) 88–116, https://doi.org/10.1016/J.WATRES.2017.04.014.
[48] V.G. Georgieva, L. Gonsalvesh, M.P. Tavlieva, Thermodynamics and kinetics of the removal of nickel (II) ions from aqueous solutions by biochar adsorbent made from agro-waste walnut shells, J. Mol. Liq. 312 (2020), https://doi.org/10.1016/j.molliq.2020.112788.
[50] N. Kannan, S. Jasmin, S. Malar, Removal of Mercury(II) Ions by Adsorption Onto Dates Nut and Commercial Activated Carbons: A Comparative Study, 2005.
[51] X. Qian, R. Wang, Q. Zhang, Y. Sun, W. Li, L. Zhang, B. Qu, A delicate method for the synthesis of high-efficiency Hg (II) the adsorbents based on biochar from corn straw biogas residue, J. Clean. Prod. 355 (2022), https://doi.org/10.1016/j.jclepro.2022.131819.
[52] C.J. Hsu, Y.H. Cheng, Y.P. Huang, J.D. Atkinson, H.C. Hsi, A novel synthesis of sulfurized magnetic biochar for aqueous Hg(II) capture as a potential method for environmental remediation in water, Sci. Total Environ. 784 (2021), https://doi.org/10.1016/j.scitotenv.2021.147240.
[53] W. Shen, Y. Fang, M. Azeem, Y. Gao, X. Li, P. Zhao, A. Ali, M. Li, R. Li, Chitosan crosslinked with polyamine-co-melamine for adsorption of Hg2+: application in purification of polluted water, Int. J. Biol. Macromol. 181 (2021) 778–785, https://doi.org/10.1016/j.ijbiomac.2021.03.166.
[56] T. Kokab, H.S. Ashraf, M.B. Shakoor, A. Jilani, S.R. Ahmad, M. Majid, S. Ali, N. Farid, R.A. Alghamdi, D.A.H. Al-Quwaie, K.R. Hakeem, Effective removal of Cr (Vi) from wastewater using biochar derived from walnut shell, Int. J. Environ. Res. Public Health 18 (2021), https://doi.org/10.3390/ijerph18189670.
[57] G. Liu, L. Zhang, R. Luo, Preparation of efficient heavy metal adsorbent based on walnut shell and adsorption for Pb(II) ions from aqueous solution, Cellulose 29 (2022) 9819–9830, https://doi.org/10.1007/s10570-022-04869-z.
[58] J.S. Cao, J.X. Lin, F. Fang, M.T. Zhang, Z.R. Hu, A new absorbent by modifying walnut shell for the removal of anionic dye: kinetic and thermodynamic studies, Bioresour. Technol. 163 (2014) 199–205, https://doi.org/10.1016/j.biortech.2014.04.046.
[59] L. Cheng, L. Sun, W. Xue, Z. Zeng, S. Li, Adsorption equilibrium and kinetics of Pb (II) from aqueous solution by modified walnut shell, Environ. Prog. Sustain. Energy 35 (2016) 1724–1731, https://doi.org/10.1002/ep.12424.
[60] J. Li, J. Ma, Q. Guo, S. Zhang, H. Han, S. Zhang, R. Han, Adsorption of hexavalent chromium using modified walnut shell from solution, Water Sci. Technol. 81 (2020) 824–833, https://doi.org/10.2166/wst.2020.165.
[61] S. Li, Z. Zeng, W. Xue, Adsorption of lead ion from aqueous solution by modified walnut shell: kinetics and thermodynamics, Environ. Technol. (UK) 40 (2019) 1810–1820, https://doi.org/10.1080/09593330.2018.1430172.